Spatiotemporal dynamics of photon echoes from continuum states in semiconductors

S. Glutsch, U. Siegner,* and D. S. Chemla
Department of Physics, University of California at Berkeley and Materials Sciences Division, Lawrence Berkeley Laboratory, Berkeley, California 94720
(Received 27 February 1995)

We study the dynamics of coherent emission of a semiconductor within the framework of the semiconductor Bloch equations, both in the time domain and in real space for various excitation conditions. We find that the spatial properties of the four-wave-mixing (FWM) response reflect the well-known temporal dynamics. For excitation high above the band edge, the FWM signal is emitted as a photon echo. This photon echo from continuum states of a semiconductor has the same dynamical properties as a photon echo from inhomogeneously broadened uncoupled two-level systems. However, unlike the case of two-level atoms, the polarization of the photon echo from the semiconductor continuum extends over macroscopic distances in real space. The implications of the large spatial extent of the photon echo polarization are discussed. In particular, we show that, in spite of the macroscopic size of the photon echo polarization, the wavelength of the exciting light can still be neglected.

I. INTRODUCTION

Photon echo experiments are a powerful tool to determine the homogeneous linewidth of an inhomogeneously broadened optical transition.[1] This experimental technique overcomes the difficulty that, in the case of inhomogeneous broadening, the dephasing-induced decay of the polarization is masked by destructive interference between the various frequency components in the inhomogeneous line. In the simplest implementation of a photon echo or four-wave-mixing (FWM) experiment, an inhomogeneously broadened optical transition is excited by two short time-delayed laser pulses. The decay of the macroscopic polarization generated by the first pulse is reversed by nonlinear interaction with the second one. This leads to the generation of a nonlinear polarization, which is the source of a time-delayed signal pulse, known as photon echo. The decay of the photon echo, with increasing time delay between the excitation pulses, yields information on the dephasing and the homogeneous linewidth.

In semiconductor physics, photon echo experiments have been widely used to study dephasing processes and the underlying scattering mechanisms in disordered systems such as mixed crystals[2–4] or quantum wells with pronounced well width fluctuations.[5,6] In this situation, extrinsic disorder gives rise to inhomogeneous broadening. For disordered semiconductors, the photon echo dynamics has been discussed in terms of uncoupled two-level systems,[7] thus neglecting Coulomb correlation.

Another approach to the photon echo phenomenon involves the continuum states of an ideal and perfectly ordered semiconductor crystal. The continuum states can be viewed as two-level systems inhomogeneously broadened in **k** space, if Coulomb correlation is neglected. Here, the inhomogeneous broadening is intrinsic to the semiconductor. For a realistic description, however, Coulomb interaction has to be included, e.g., in the framework of the semiconductor Bloch equations.[8] In a pioneering work, Lindberg *et al.*[9] have solved the semiconductor Bloch equations for excitation at the band edge of a two-band semiconductor. Their numerical results show that a photon echo is emitted in this situation. Later on, the theory was refined to take into account the valence band structure of a real semiconductor,[10] and the simultaneous influence of extrinsic disorder and Coulomb correlation.[11] Experimentally, the intrinsic photon echo from the semiconductor continuum states has been observed in bulk semiconductors[12] and quantum wells.[13]

The theoretical interest, so far, has been focused on the temporal behavior of the intrinsic photon echo from semiconductor continuum states rather than on the spatial behavior. One aspect of the space dependence is the propagation of the fields. Very recently, the consequences of polariton effects in four-wave-mixing experiments have been studied by Bakker and Kurz.[14] In the present paper, we focus on the dependence of the polarization on the relative coordinate.

We have studied the spatially resolved polarization within the framework of the semiconductor Bloch equations,[8] at fixed time delays and fixed real times. Furthermore, we have calculated the spatially integrated nonlinear polarization generated in a FWM experiment both as a function of real time for fixed time delays (time-resolved FWM: TR FWM) and integrated over the real time as a function of the time delay (time-integrated FWM: TI FWM). Experimentally, the TR FWM signal can be obtained by upconversion of the FWM signal pulse with a reference pulse.

In order to be more general and to characterize the intrinsic photon echo in comparison to the FWM response of the homogeneously broadened exciton transition, we have calculated the FWM response in time and space for various excitation conditions. For excitation of the exci-

0163-1829/95/52(7)/4941(10)/$06.00

ton only, we rederive the well-known exciton dynamics in the time domain.[15–19] As expected, we find a free polarization decay of the excitonic polarization, with a slow rise due to exciton-exciton interaction. In real space, this is reflected by an exciton polarization, which is essentially confined to a volume of the order of the exciton Bohr radius.

Moving the excitation energy to the band edge, bound and unbound states of the exciton Rydberg series are excited simultaneously.[20,21] Here, the expected quantum beating between the $1s$ exciton and higher excitonic states is found in the time domain. In this situation, the polarization is no longer confined in space, but starts to expand due to the excitation of continuum states.

Only continuum states are excited for excitation high above the band edge. The TR FWM signal now shows all the characteristics of a photon echo, i.e., it is emitted with a time delay that equals the time delay between the excitation pulses, and is corrected by the influence of the dephasing and the finite width of the pulses. We further demonstrate that the dynamics of the photon echo are not changed by Coulomb correlation. The temporal evolution of photon echo from continuum states of a semiconductor is very similar to that of the photon echo from two-level systems. In real space, the delayed emission of the echo signal manifests itself by expansion and subsequent contraction of the polarization. At the maximum of its spatial extent, the polarization occupies a *macroscopic* volume. This has important consequences for the dephasing. The macroscopic size of the photon echo polarization also raises the question of whether it is still valid to neglect the finite wavelength of the excitation pulses, which is the common practice in the treatment of FWM experiments. We show that the wavelength can still be neglected in this situation.

The paper is organized as follows: to introduce our notation, in Sec. II, we first summarize the treatment of photon echoes for the model of uncoupled two-level systems; the analytical and numerical results for the spatial and temporal dynamics of excitons and continuum states in semiconductors as well as a discussion of the implications of the finite wavelength of the excitation laser pulses in view of the macroscopic extent of the polarization in a photon echo experiment are presented in the main part of the paper, Sec. III; our conclusions are given in Sec. IV.

II. INDEPENDENT TWO-LEVEL SYSTEMS

The basic mechanism of photon echo dynamics can be explained by the model of inhomogeneously broadened and uncoupled two-level systems.[7] Such an idealized model, however, is only appropriate for a qualitative description of a real configuration. In this section, we briefly summarize the results for two-level systems and introduce our notation. The analytical results for two-level systems will be compared with the full numerical results for a semiconductor in the following section.

We consider a set $\{\lambda\}$ of independent two-level systems with transition energies $\hbar\omega^{(\lambda)}$, equally distributed in a normalization volume Ω. Assuming that each of the two-level systems is coupled to the electric field E by a dipole matrix element μ, the equation of motion for the density matrices $N^{(\lambda)}$ is given by the von Neumann equation,

$$i\hbar \frac{d}{dt} N^{(\lambda)}(t) = \left[H^{(\lambda)}(t) , N^{(\lambda)}(t) \right] , \tag{1}$$

where

$$H^{(\lambda)}(t) = \begin{pmatrix} +\frac{1}{2}\hbar\omega^{(\lambda)} & -\mu E(t) \\ -\mu^* E^*(t) & -\frac{1}{2}\hbar\omega^{(\lambda)} \end{pmatrix} ;$$

$$N^{(\lambda)}(-\infty) = \mathrm{diag}(0 , 1) .$$

We have assumed zero temperature and no dephasing in order to obtain an analytical formula for the FWM signal. The influence of a finite dephasing time T_2 will be taken into account later. Consistent with the assumption of independent systems, local field effects are neglected. The influence of dephasing will be discussed later. The polarization,

$$P(t) = \mu^* \frac{1}{\Omega} \sum_{\lambda} n_{12}^{(\lambda)}(t) ,$$

is given by the number of dipoles per unit volume.

Equation (1) can be solved analytically in arbitrary orders in the field strength.[7] The first order yields

$$P^{(1)}(t) = -\frac{|\mu|^2}{i\hbar} \frac{1}{\Omega} \sum_{\lambda} \int_{-\infty}^{t} dt' \, e^{-i\omega^{(\lambda)}(t-t')} E(t') .$$

Introducing the Fourier transform of E,

$$\tilde{E}(\omega) = \int_{-\infty}^{+\infty} dt \, e^{+i\omega t} E(t) ,$$

and P, we find for the linear optical susceptibility $\tilde{\chi}(\omega) = \tilde{P}(\omega)/[\varepsilon_0 \tilde{E}(\omega)]$ that

$$\mathrm{Im}\,\tilde{\chi}(\omega) = \frac{|\mu|^2}{\varepsilon_0} \frac{1}{\Omega} \sum_{\lambda} \frac{\pi}{\hbar} \delta(\omega - \omega^{(\lambda)}) = \frac{\pi |\mu|^2}{\varepsilon_0 \hbar} \tilde{D}(\omega) , \tag{2}$$

where $\tilde{D}$ is the density of states of an ensemble of two-level systems with energies $\hbar\omega^{(\lambda)}$.

In order to calculate the FWM signal, we have to take into account the dependence of the field strength on the space coordinate. We assume an electric field consisting of two pulses nonoverlapping in time with a time delay Δt between the first and the second one:

$$E(\mathbf{r}, t) = E_1(t) \, e^{+i\mathbf{K}_1 \cdot \mathbf{r}} + E_2(t) \, e^{+i\mathbf{K}_2 \cdot \mathbf{r}} , \tag{3}$$

$$\mathrm{supp}E_1 \cap \mathrm{supp}E_2 = \emptyset ;$$

$$E_1(t) = E(t) ; \quad E_2(t) = E(t - \Delta t) .$$

Here, "supp$f$" means the support of a function f, i.e., the interval where f is different from zero. As an exact re-

sult, the FWM signal, i. e., the contribution to the third-order polarization proportional to $E_2^2 E_1^*$ (in the sense of a variational derivative), is emitted in the direction $2\mathbf{K}_2 - \mathbf{K}_1$ and its amplitude is given by

$$P^{(3)}(t) = -2\frac{|\mu|^4}{(i\hbar)^3}\frac{1}{\Omega}\sum_\lambda \int_{-\infty}^{t} dt_3 \int_{-\infty}^{t_3} dt_2 \int_{-\infty}^{t_2} dt_1 \times E_2(t_3)E_2(t_2)E_1^*(t_1)e^{-i\omega^{(\lambda)}(t-t_3-t_2+t_1)}. \quad (4)$$

Based on our assumptions (3), for $t > \max(\mathrm{supp}E_2)$ Eq. (4) considerably simplifies to

$$P^{(3)}(t) = -\frac{|\mu|^4}{(i\hbar)^3}\frac{1}{\Omega}\sum_\lambda e^{-i\omega^{(\lambda)}(t-2\Delta t)} \times \tilde{E}(\omega^{(\lambda)})\left|\tilde{E}(\omega^{(\lambda)})\right|^2. \quad (5)$$

The latter sum can be evaluated using the density of states introduced in Eq. (2). For an absorption coefficient that is constant in the frequency range of interest, i. e., $\mathrm{Im}\,\chi(\omega) \equiv \mathrm{Im}\,\chi(\bar{\omega})$, where $\bar{\omega}$ is the center frequency of the pulse, we obtain the analytical result:

$$P^{(3)}(t) = \frac{2i\varepsilon_0|\mu|^2}{(i\hbar)^2}\,\mathrm{Im}\,\tilde{\chi}(\bar{\omega}) \int_{-\infty}^{+\infty} dt' \int_{-\infty}^{+\infty} dt'' \times E(t-2\Delta t-t')\,E(t'-t'')\,E^*(-t''). \quad (6)$$

To simplify the notation, we define the convolution "$*$" by

$$[f(.)*g(.)](\vec{\xi}) = \int d^m\vec{\xi}'\, f(\vec{\xi}-\vec{\xi}')\,g(\vec{\xi}'),$$

where $\vec{\xi}$ is a vector in an m-dimensional space. The convolution satisfies the following relations: $f*g = g*f$ and $f*(g*h) = (f*g)*h$. With this definition, Eq. (6) reads

$$P^{(3)}(t) = \frac{2i\varepsilon_0|\mu|^2}{(i\hbar)^2}\,\mathrm{Im}\,\tilde{\chi}(\bar{\omega}) \times\left[E(.)*E(.)*E^*(-.)\right](t-2\Delta t).$$

Now we consider a Gaussian pulse with a width σ, i. e., $E(t) = \bar{E}\exp\left[-t^2/(2\sigma^2)\right]e^{-i\bar{\omega}t}$. For $\Delta t \gg \sigma$, the condition of nonoverlapping pulses is fulfilled and the evaluation of Eq. (6) yields a polarization of a Gaussian temporal profile with a width $\sqrt{3}\sigma$, centered at $2\Delta t$. This polarization is the source of the photon echo.

A simple analytical formula, like Eq. (6), cannot be given for the polarization if we take into account a finite dephasing time $T_2 = 1/\gamma$. From an approximate treatment, we obtain an additional shift of $-4\gamma\sigma^2 + O(\gamma^2\sigma^3)$ for the polarization, i. e., the polarization is centered now at $2\Delta t - 4\gamma\sigma^2 + O(\gamma^2\sigma^3)$. The shift can be of the order of the pulse width and has to be accounted for a quantitative analysis of photon echo experiments.

III. TWO-BAND SEMICONDUCTOR

If Coulomb interaction is neglected a semiconductor can be viewed as an ensemble of inhomogeneously broadened and uncoupled two-level systems in $\mathbf{k}$ space. The FWM signal from a semiconductor exhibits the properties of a photon echo in this approximation, as shown in the previous section. However, it is known that neglecting or treating the Coulomb interaction as a small perturbation is an inadequate description. This is already obvious from an inspection of the first-order polarization, where Coulomb effects produce excitonic features that drastically change the linear absorption in a relatively large spectral region around the absorption edge.

The semiconductor Bloch equations[8] provide a more sophisticated description of the interaction of light with a semiconductor. This formalism includes Coulomb correlation within the Hartree-Fock approximation. In this section, we study the FWM response of a semiconductor within the framework of the semiconductor Bloch equations for excitation at the $1s$ exciton, between the $1s$ exciton and the absorption edge, and far in the continuum. Special emphasis is put on the relationship between spatial and temporal behavior, and on the comparison to the noninteracting case where Coulomb correlation is neglected. In Sec. III A, we establish the semiconductor Bloch equation in real space and derive a hierarchy of differential equations that allows us to successively calculate the third-order polarization. Numerical solutions are discussed in Sec. III B. We also show that the Coulomb potential contributes significantly to the intensity of the photon echo. The temporal line shape of the signal, however, is hardly changed by Coulomb correlation. This is due to the fact that the electron-hole pair amplitude of interacting particles is essentially determined by multiplying the amplitude of the noninteracting system by a complex factor which slowly varies in space and time.

A. Semiconductor Bloch equations in real space

Within the Hartree-Fock approximation, the time dependence of the density matrix in a semiconductor is described by the semiconductor Bloch equations. Their formulation in real space is

$$i\hbar\frac{\partial}{\partial t}N(\mathbf{r},t) = \left[H(.,t)*, N(.,t)\right](\mathbf{r}) + i\hbar\left(\frac{\partial N(\mathbf{r},t)}{\partial t}\right)_{\mathrm{ext}},$$

where

$$H(\mathbf{r},t) = \begin{pmatrix} -\frac{\hbar^2}{4m}\Delta & -\mu E(t) \\ -\mu^* E^*(t) & +\frac{\hbar^2}{4m}\Delta \end{pmatrix}\delta(\mathbf{r}) - V(\mathbf{r})\left[N(\mathbf{r},t) - N(\mathbf{r},-\infty)\right], \quad (7)$$

$$\left(\frac{\partial n_{ij}(\mathbf{r},t)}{\partial t}\right)_{\mathrm{ext}} = \begin{cases} 0 & \text{for } i=j \\ -\gamma\, n_{ij}(\mathbf{r},t) & \text{for } i\neq j, \end{cases}$$

$$m = \frac{m_e m_h}{m_e+m_h}; \quad V(\mathbf{r}) = \frac{e^2}{4\pi\varepsilon_0\varepsilon r};$$

$$N(\mathbf{r},-\infty) = \mathrm{diag}(0,1)\,\delta(\mathbf{r}).$$

Here, ε_0 is the vacuum dielectric constant and ε is the static dielectric constant of the semiconductor. We have assumed that relaxation and recombination can be neglected in comparison to dephasing, i.e., $T_1 \gg T_2 = 1/\gamma$. We expect from the last section that the changes due to a finite relaxation time are small.

Now, we successively evaluate Eq. (7) up to the third order in the field strength. We use the notation $n = n_{cc}$ and $\psi = n_{cv}$. The latter quantity is known as the electron-hole pair amplitude and gives rise to the polarization of the semiconductor.

We have to solve the set of differential equations,

$$i\hbar \frac{\partial}{\partial t} \psi^{(1)}_{1,2}(\mathbf{r},t) = \left[-\frac{\hbar^2}{2m}\Delta - V(\mathbf{r}) - i\hbar\gamma \right] \psi^{(1)}_{1,2}(\mathbf{r},t) - \mu E_{1,2}(t)\,\delta(\mathbf{r}) \,, \tag{8a}$$

$$i\hbar \frac{\partial}{\partial t} n^{(2)}(\mathbf{r},t) = \left\{ \left[-\mu E_2(t)\,\delta(.) - V(.)\,\psi^{(1)}_2(.,t) \right] * \psi^{(1)*}_1(.,t) \right\}(\mathbf{r}) - \left\{ \psi^{(1)}_2(.,t) * \left[-\mu^* E^*_1(t)\,\delta(.) - V(.)\,\psi^{(1)*}_1(.,t) \right] \right\}(\mathbf{r}) \,, \tag{8b}$$

$$i\hbar \frac{\partial}{\partial t} \psi^{(3)}(\mathbf{r},t) = \left[-\frac{\hbar^2}{2m}\Delta - V(\mathbf{r}) - i\hbar\gamma \right] \psi^{(3)}(\mathbf{r},t) + 2\left\{ \left[-V(.)\,n^{(2)}(.,t) \right] * \psi^{(1)}_2(.,t) \right\}(\mathbf{r}) - 2\left\{ \left[-\mu E_2(t)\,\delta(.) - V(.)\,\psi^{(1)}_2(.,t) \right] * n^{(2)}(.,t) \right\}(\mathbf{r}) \,, \tag{8c}$$

for functions E_1, E_2 defined in Eq. (3), and initial conditions $\psi^{(1)}_{1,2}(\mathbf{r},-\infty) = n^{(2)}(\mathbf{r},-\infty) = \psi^{(3)}(\mathbf{r},-\infty) \equiv 0$. The only input parameters are the width of the Gaussian pulse σ, the time delay Δt, and the homogeneous broadening $\hbar\gamma$, fixed at $0.2\,E_B$ throughout the paper, where E_B is the exciton binding energy. The third-order polarization, $P^{(3)}(t) = \mu^* \psi^{(3)}(\mathbf{0},t)$, is not directly accessible in experiments. However, the TR FWM signal $\mathrm{TR}(t) \propto |P^{(3)}(t)|^2$ for a fixed time delay and the TI FWM signal $\mathrm{TI}(\Delta t) \propto \int_{-\infty}^{+\infty} dt\, |P^{(3)}(t)|^2$ can be determined experimentally.

The above equations show that Coulomb interaction affects the dynamics of the FWM signal in two ways: (i) The potential V is part of the differential operator in Eqs. (8a) and (8c). This *Coulomb enhancement* is responsible for the creation of bound states, i.e., excitons, and modifies the continuum wave functions in the neighborhood of the origin $\mathbf{r} = \mathbf{0}$. (ii) The Coulomb potential contributes to the source terms of Eqs. (8b) and (8c). This is known as *polarization interference*.[8]

In the linear spectrum, the Coulomb enhancement manifests itself by the formation of exciton transitions below the band edge and by a significant increase of the continuum absorption (Sommerfeld factor) over a spectral region of the order of tens of E_B.

Polarization interference changes the nonlinear optical properties of a semiconductor. This is the dominant term in the FWM signal for excitonic states that leads to deviations from a strictly exponential decay of the TR FWM signal and to a nonvanishing signal for negative time delays.[15–19] The influence of the Coulomb interaction on the FWM signal from the continuum has not been studied. This point will be addressed in the next subsection. Intuitively, we expect an amplification of the signal due to Coulomb enhancement, but only a small effect due to polarization interference in the case of the continuum.

B. Numerical results

Since analytical solutions for the full problem are not available, we integrate the differential equations (8a)–(8c) numerically. All explicit results are given in excitonic units, i.e., the binding energy $E_B = \frac{1}{2}\, me^4/[(4\pi\varepsilon_0\varepsilon)^2\hbar^2]$ of the exciton and the Bohr radius $a_B = 4\pi\varepsilon_0\varepsilon\,\hbar^2/(me^2)$. We use the parameters of gallium arsenide, which are $E_B \approx 4.7\,\mathrm{meV}$, $a_B \approx 10\,\mathrm{nm}$, and $\hbar/E_B \approx 140\,\mathrm{fs}$.[22]

The linear optical susceptibility $\tilde{\chi}$ is related to the first-order polarization, $P^{(1)}(t) = \mu^* \psi^{(1)}(\mathbf{0},t)$, by

$$\tilde{\chi}(\omega) = \frac{\tilde{P}^{(1)}(\omega)}{\varepsilon_0 \tilde{E}(\omega)} \,.$$

Although this equation has analytical solutions,[23] we choose to solve Eq. (8a) numerically for reasons that become clear in the next paragraph. The imaginary part of the optical susceptibility, taking into account Coulomb effects, is depicted as solid line in Fig. 1. The lower solid line in Fig. 1 shows the imaginary part of the optical susceptibility, neglecting Coulomb effects. The numerical solutions are in excellent agreement with the analytical ones. The comparison of the absorption spectra demonstrates that, even far in the continuum, the Coulomb enhancement is important. At $\hbar\omega = 10\,E_B$ the absorption is still more than twice as high for the interacting system, compared to the free-particle result.

In the remaining part of this subsection, we show how the spatial properties of the electron-hole-pair amplitude ψ are related to the temporal behavior of the third-order polarization, i.e., to the FWM signal. It is worthwhile to recall that only the polarization at $\mathbf{r} = \mathbf{0}$ is monitored in an optical experiment. Thus, the FWM signal reveals only the electron-hole pair amplitude at zero radius, while the spatially resolved polarization provides a more complete picture.

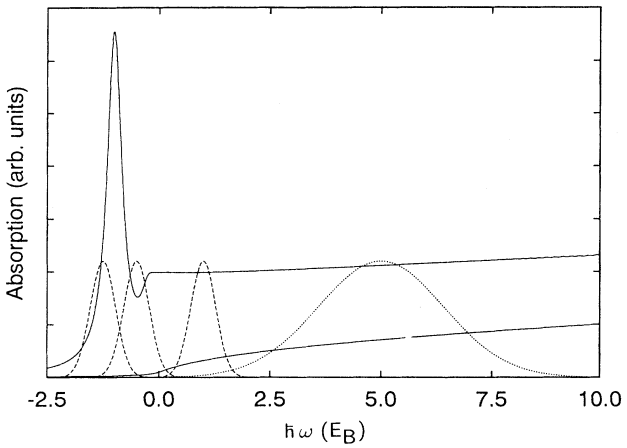

FIG. 1. Solid lines: Optical absorption $\mathrm{Im}\,\chi(\omega)$ vs energy $\hbar\omega$ for interacting and noninteracting particles. The dephasing rate $\hbar/T_2$ is $0.2\,E_B$. Dashed lines: Power spectra $|\tilde{E}|^2$ of Gaussian excitation pulses with width $\sigma = 2.5\,\hbar/E_B$ centered at energies $\hbar\bar{\omega} = -1.25$, -0.5, and $+1\,E_B$. Dotted line: Excitation spectrum with $\sigma = 0.5\,\hbar/E_B$ centered at $\hbar\bar{\omega} = 5\,E_B$.

We have solved the set of Eq. (8) for various excitation conditions. The spectral intensities $|\tilde{E}(\omega)|^2$ of the exciting pulse are shown by dashed and dotted curves in Fig. 1.

First, we consider the real-space dependence of the linear polarization as the spectrum of the excitation laser is shifted from the exciton to the continuum (cf. dashed excitation spectra in Fig. 1). In Fig. 2, the evolution of the first-order electron-hole pair amplitude is shown for excitation at the exciton resonance, between the $1s$ exciton and the continuum, and in the continuum. The normalized functions $r^2\,|\psi_1^{(1)}(\mathbf{r},t)|^2$ are plotted versus radius r for different times $t = 2.5,\ 5,\ 7.5,\ \ldots,\ 22.5\,\hbar/E_B$. The center frequency of the pulse is $\hbar\bar{\omega} = -1.25$ (a), -0.5 (b), and $+1\,E_B$ (c), respectively.

For excitation at the exciton resonance [Fig. 2(a)], the spatially resolved polarization has essentially the shape of the exciton wave function. There is a small contribution from higher excitonic states at early times, i. e., right after the polarization has been created. This part becomes larger if the whole Rydberg series is excited [Fig. 2(b)]. The contribution from higher excitonic states expands with increasing time. The main contribution, however, still has the form of the $1s$ exciton wave function even for excitation of the whole Rydberg series.

A different situation is encountered when the continuum is excited [Fig. 2(c)]. The pulse spectrum is chosen such that virtually no overlap occurs with discrete states (cf. Fig. 1). Figure 2(c) shows that the polarization is created in a narrow region around $\mathbf{r} = \mathbf{0}$, but that it expands rapidly. At later times, the polarization occupies a large volume. For example, the effective diameter d of the polarization in GaAs increases to about $1\,\mu$m within 3000 fs, i. e., the polarization extends over macroscopic distances. As a consequence of the spatial dynamics, for excitation of the continuum the first-order polarization $P^{(1)}$, which is proportional to $\psi^{(1)}(\mathbf{0},t)$, shows an instantaneous temporal response and decays on the time scale of the exciting pulse.

The function $\psi_1^{(1)}$ is responsible for the creation of the elements $n^{(2)}$ and $\psi^{(3)}$ of the density matrix. This process is demonstrated in Fig. 3 where the function $r^2\,|\psi^{(3)}(\mathbf{r},t)|^2$ is shown for times $t = 20,\ 22.5,\ 25,\ \ldots,\ 40\,\hbar/E_B$. The time delay Δt between the first and the second pulse is fixed at $16\,\hbar/E_B$. The other parameters are the same as in Fig. 2.

Again, for excitation at the exciton resonance [Fig. 3(a)], the electron-hole-pair amplitude resembles the exciton wave function, but the deviations are larger than in the first order. The source term for the third

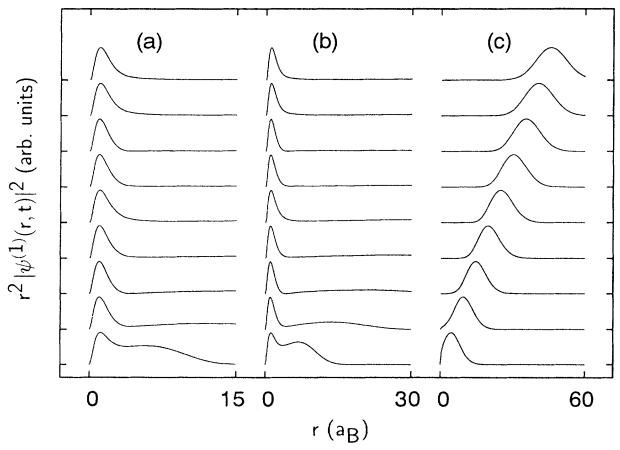

FIG. 2. Normalized functions $r^2\,|\psi^{(1)}(\mathbf{r},t)|^2$ vs radius r at times $t = 2.5,\ 5,\ 7.5,\ \ldots,\ 22.5\,\hbar/E_B$ (from bottom to top). The excitation spectra are centered at $\hbar\bar{\omega} = -1.25$ (a), -0.5 (b), and $+1\,E_B$ (c). The duration of the excitation pulses is $\sigma = 2.5\,\hbar/E_B$ and the dephasing rate is $\hbar/T_2 = 0.2\,E_B$.

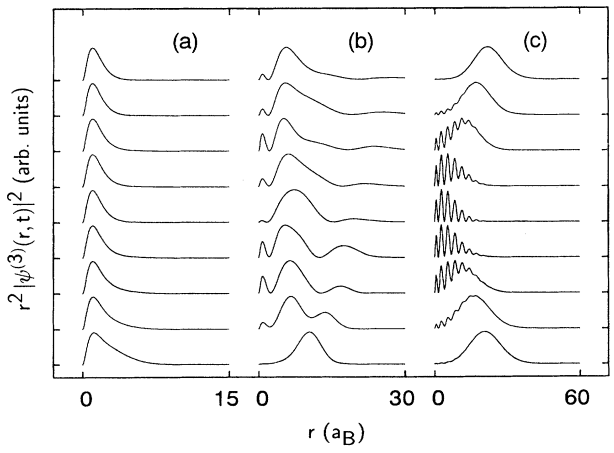

FIG. 3. Normalized functions $r^2\,|\psi^{(3)}(\mathbf{r},t)|^2$ vs radius r at times $t = 20,\ 22.5,\ 25,\ \ldots,\ 40\,\hbar/E_B$ (from bottom to top). The excitation spectra are centered at $\hbar\bar{\omega} = -1.25$ (a), -0.5 (b), and $+1\,E_B$ (c). The time delay Δt is $16\,\hbar/E_B$. The width of the exciting pulses and the dephasing rate are the same as in Fig. 2.

order (8c) is no longer proportional to a Dirac function in space, $\delta(\mathbf{r})$, as it is the case for the first order (8a), but is delocalized due to Coulomb interference and the finite extension of $n^{(2)}$.

A remarkable difference between first and third order can be observed for excitation between the exciton and the continuum [Fig. 3(b)]. Now, a much larger portion of the third-order spatially resolved polarization is created at a finite radius. It moves towards $\mathbf{r} = \mathbf{0}$, where a $1s$-exciton-like function is formed at later times. This function continuously interferes with higher excitonic states, which form a quasicontinuum. Parts of the wave packet move away from the point $\mathbf{r} = \mathbf{0}$.

A more regular behavior is observed for the continuum response [Fig. 3(c)]. Essentially, no part of the third-order polarization is created at $\mathbf{r} = \mathbf{0}$. In the course of time, the wave packet moves as a whole to the point $\mathbf{r} = \mathbf{0}$, where interference takes place between the incoming and the reflected part. Later, the volume occupied by the wave packet increases again.

The third-order spatially resolved polarization is related to the four-wave-mixing signal, which is proportional to $|\psi^{(3)}(\mathbf{0}, t)|^2$. In Fig. 4, the TR FWM signal is plotted versus time. The solid, dashed, and dotted lines correspond to the excitation conditions (a), (b), and (c), respectively, of Figs. 2 and 3.

The FWM signal from the exciton (solid line) can be well described by $\mathrm{TR}(t) = \mathrm{const} \times (t - \Delta t)^2 \exp(-2\gamma t)$ for $t > \Delta t$. It shows the expected slow rise and an exponential decay in the long-time limit. Only a slight oscillation is observed, which stems from interference with higher excitonic states. For varying time delay, the position of the maximum, $t_{\max}$ is approximately given by $t_{\max}(\Delta t) = \Delta t + 1/\gamma$. The slow rise of the TR FWM signal is due to polarization interference, which dominates the generation of the third-order polarization.[17–19]

The signal maximum shows an additional delay for excitation between exciton and continuum (dashed line), because the spatially resolved third-order polarization is mainly created at $r > 0$ and needs a certain time to reach the point $\mathbf{r} = \mathbf{0}$. The signal is characterized by an irregular and nonperiodic beating, which can be explained by interference between the excitonic contribution and contributions with a larger spatial extent.

An instantaneous FWM response is not observed for excitation in the continuum (dotted line in Fig. 4), since the third-order spatially resolved polarization is created at $r > 0$. A photon echo is emitted at the time $t = 2\Delta t$ when the wave packet has reached the point $\mathbf{r} = \mathbf{0}$. As expected, the time-resolved echo signal drops rapidly and contains no slowly decaying contributions. Importantly, the qualitative behavior of the photon echo is not changed even if we assume $\hbar\gamma = 0$. This is striking in contrast to the FWM signal from the exciton, where the neglect of dephasing results in a diverging signal. Recalling that the divergence of the excitonic FWM signal in this situation is due to polarization interference, this indicates that polarization interference does not play a significant role for the FWM response from semiconductor continuum states.

The dephasing and the finite pulse width lead to a noticeable shift of the photon echo pulse from the ideal position $t = 32\,\hbar/E_B$. The maximum of the photon echo is found at $t_{\max} = 26.4\,\hbar/E_B$, in good agreement with the value $2\,\Delta t - 4\gamma\,\sigma^2 = 27\,\hbar/E_B$ predicted by the model of a two-level system in Sec. II. The overall behavior of the maximum position as function of the delay is $t_{\max}(\Delta t) \sim 2\Delta t + c$ for $t \to +\infty$, where $c \approx -4\,\gamma\,\sigma^2$, as found from the numerical data. This shows, once more, the difference to the excitonic polarization decay.

The TI FWM signals are shown in Fig. 5. We find, for excitation at the exciton (solid line), that $\mathrm{TI}(\Delta t) \sim \mathrm{const} \exp(-2\,\gamma\,\Delta t)$ for $t \to +\infty$ and $\mathrm{TI}(\Delta t) \sim \mathrm{const} \exp(+4\,\gamma\,\Delta t)$ for $t \to -\infty$, in agreement with earlier works.[15,16] For excitation between exciton and con-

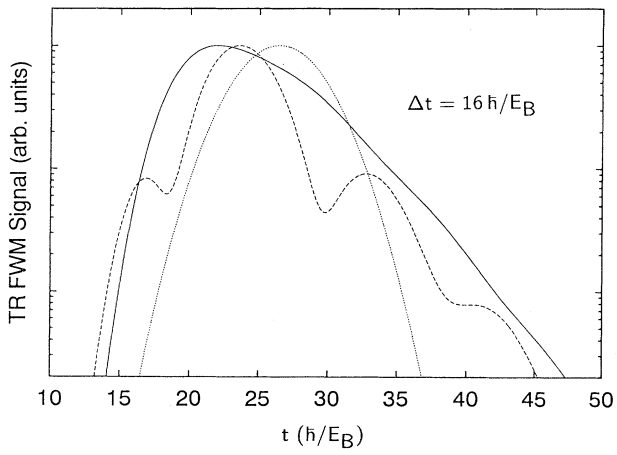

FIG. 4. Normalized TR FWM signals $\mathrm{TR}(t)$ vs time t, for the same excitation conditions as in Fig. 3. Solid line: Excitation centered at $\hbar\bar{\omega} = -1.25\,E_B$. Dashed line: Excitation centered at $\hbar\bar{\omega} = -0.5\,E_B$. Dotted line: Excitation centered at $\hbar\bar{\omega} = +1\,E_B$. The signal from the continuum is about 500 times weaker than that from the exciton.

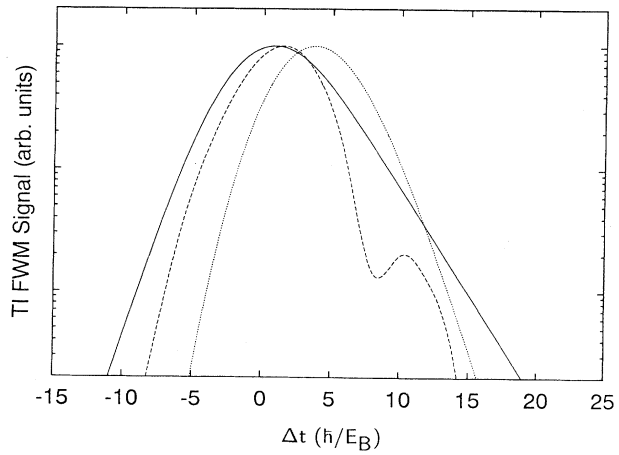

FIG. 5. TI FWM signals $\mathrm{TI}(\Delta t)$ vs time delay Δt for the same excitation conditions as in Fig. 4. Solid line: Excitation centered at $\hbar\bar{\omega} = -1.25\,E_B$. Dashed line: Excitation centered at $\hbar\bar{\omega} = -0.5\,E_B$. Dotted line: Excitation centered at $\hbar\bar{\omega} = +1\,E_B$.

tinuum (dashed line), the expected quantum beating is observed. The beating is less pronounced than in the corresponding TR signal, since the integration averages over the quantum beat modulation of the TR FWM signal. The TI signal from the continuum is proportional to $\exp(-4\gamma\Delta t)$, as in the case of inhomogeneously broadened and independent two-level systems.

Summarizing the above discussion, we note that the temporal dynamics of the FWM signal is reflected by the spatial dynamics of the polarization. In particular, our results demonstrate that the delayed emission of the photon echo corresponds in real space to expansion of the first-order and subsequent contraction of the third-order polarization. In contrast, the third-order polarization of the exciton is essentially created at $\mathbf{r} = \mathbf{0}$. As a consequence, the excitonic FWM signal starts to rise immediately after the excitation.

Now, we focus on the comparison between the photon echo dynamics in the interacting and noninteracting system, i.e., we treat the semiconductor with and without Coulomb correlation. For this purpose, we choose a much shorter excitation pulse than previously, with the width $\sigma = 0.5\,\hbar/E_B$, whose spectrum is centered far in the continuum at the energy $\hbar\bar{\omega} = 5\,E_B$ (cf. dotted excitation spectrum in Fig. 1). The time delay is $\Delta t = 10\,\hbar/E_B$. The pulse spectrum covers a large region of the continuum absorption under these excitation conditions. We study the functions $r\,\mathrm{Re}\,\psi_1^{(1)}(\mathbf{r},t)$ and $r\,\mathrm{Re}\,\psi^{(3)}(\mathbf{r},t)$ in order to obtain information about the amplitude and the phase. For reasons of graphic representation, both functions are multiplied by the factor $\exp(+\gamma t)$ to compensate the exponential decay due to dephasing. The influence of the homogeneous broadening $\hbar\gamma$ is thus completely eliminated for the first-order polarization. This is not the case in the third order, since the homogeneous broadening has an effect on the delay of the photon echo as discussed in Sec. II.

In Fig. 6, the first-order spatially resolved polarization is shown for interacting (solid line) and noninteracting (dashed line) particles at times $t = 0$ (a), 5 (b) 10 (c), and $15\,\hbar/E_B$ (d). The free-particle result is multiplied by a factor 1.74. We observe wave packets with a slowly varying amplitude, but a rapidly changing phase. Surprisingly, for $r \geq 10\,a_B$, the first-order spatially resolved polarization of the interacting system is nearly given by multiplication of the free-particle result with a constant complex factor. This result is by no means trivial because the comparison of the linear spectra (cf. Fig. 1) reveals an essential influence of the Coulomb interaction both on the magnitude and on the functional form of the absorption profile. The reason for the small difference between the free-particle result and the result for the interacting system is that the spherical symmetric eigenfunctions of the hydrogen problem are asymptotically equal to those of free particles (up to a phase factor) and that the Coulomb enhancement takes place only in a small region around $\mathbf{r} = \mathbf{0}$. This effect should be even more pronounced for a short-range potential, i.e., when screening is important.

The function $r\,\mathrm{Re}\,\psi^{(3)}(\mathbf{r},t)$ is plotted in Fig. 7 at times $t = 10$ (a), 15 (b), 20 (c), and $25\,\hbar/E_B$ (d) for the same parameters as in Fig. 6. The time delay is $\Delta t = 10\,\hbar/E_B$. Here, the free-particle solution is multiplied by 5.6. The third-order polarization is created at the location of $\psi_1^{(1)}(\mathbf{r},\Delta t)$ [cf. Fig. 6(c) where $t = 10\,\hbar/E_B$] and contracts with increasing time. It reaches its smallest extent at $t = 2\,\Delta t$, where the photon echo is emitted. The amplitude of the signal from the interacting system is about 125 more intense compared to the noninteracting case. The radius increases again for $t > 2\,\Delta t$. The wave packets at time $t > 2\,\Delta t$ are very similar to those at early times t.

Figure 8 shows the time-resolved (a) and time-integrated (b) FWM signals for the same excitation conditions as in Figs. 6 and 7. The *normalized* TR FWM signals are compared for interacting particles (solid line),

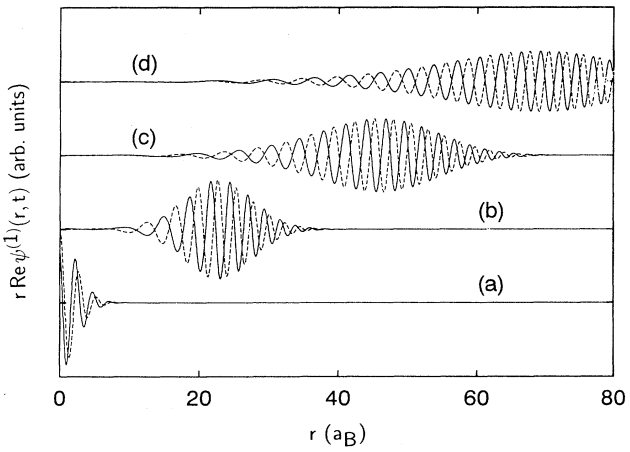

FIG. 6. Function $r\,\mathrm{Re}\,\psi^{(1)}(\mathbf{r},t)$ vs radius r at times $t = 0$ (a), 5 (b), 10 (c), and 15 (d) $\hbar/E_B$ for interacting (solid line) and noninteracting particles (dashed line, multiplied by a factor 1.74). The excitation pulses have the width $\sigma = 0.5\,\hbar/E_B$ and are centered at the energy $\hbar\bar{\omega} = 5\,E_B$. The dephasing rate is $\hbar/T_2 = 0.2\,E_B$.

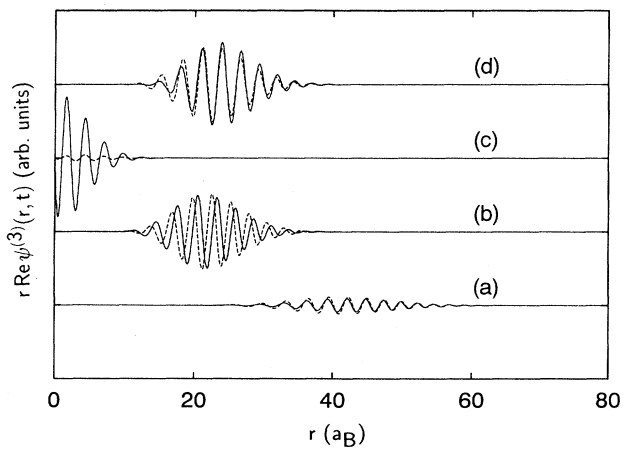

FIG. 7. Function $r\,\mathrm{Re}\,\psi^{(3)}(\mathbf{r},t)$ vs radius r at times $t = 10$ (a), 15 (b), 20 (c), and $25\,\hbar/E_B$ for interacting (solid line) and noninteracting particles (dashed line, multiplied by a factor 5.6). The time delay is $\Delta t = 10\,\hbar/E_B$. The other excitation conditions and the dephasing rate are the same as in Fig. 6.

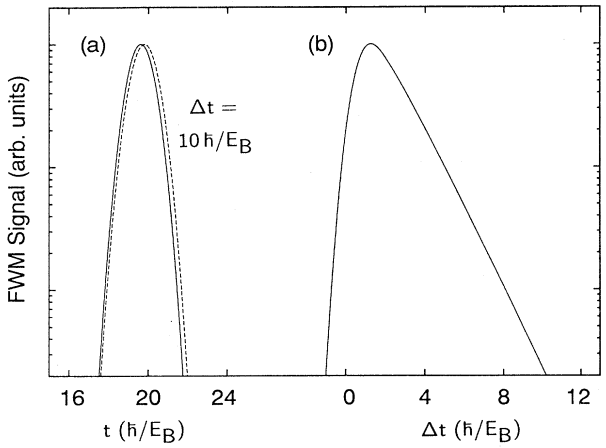

FIG. 8. FWM signals for the excitation conditions of Fig. 7. (a) TR FWM signal TR(t) vs time t for interacting particles (solid line) and noninteracting particles (dashed line). (b) TI FWM signal TI(Δt) vs time delay Δt for interacting particles.

interaction-free particles (dashed line), and independent two-level systems (data not shown in Fig. 8). Since the pulse is much shorter in this calculation than in the one shown in Fig. 4, the position of the photon echo is much closer to $2\Delta t$. There is no difference between the *normalized* TR FWM signals from the interacting and the noninteracting system besides a small shift of about $0.2\,\hbar/E_B$. The TI FWM signal [Fig. 8(b)] from the interacting system decays with the excitation pulse for negative time delays Δt in the case of continuum excitation. Since polarization interference causes a finite FWM signal at negative time delays if the exciton is excited, this result confirms that polarization interference does not significantly affect the dynamics of continuum excitations in a semiconductor. For positive time delay, we observe the expected relation $\mathrm{TI}(\Delta t) \sim \mathrm{const} \times \exp(-4\gamma\,\Delta t)$ for $\Delta t \to +\infty$.

We, finally, note that no difference can be observed between the free-particle result and the analytical solution for the two-level-system model in Sec. II. This confirms our predictions from Sec. II, because of the one-to-one correspondence of free particles and independent two-level systems. The next-order contribution to $t_{\max}$ is, in fact, extremely small since $\gamma^2\,\sigma^3 = 0.001\,25$.

The numerical results shown in Figs. 6–8 demonstrate that the semiconductor continuum has essentially the dynamic properties of a system of noninteracting particles. In particular, the functions $\psi^{(1)}$ and $\psi^{(3)}$ for the interacting system are obtained by multiplication of the free-particle result with a constant factor. Although the FWM signals for interacting and noninteracting systems have very different amplitudes, their temporal line shape is almost the same. This line shape is, essentially, determined by the solution for independent two-level systems. Whereas polarization interference dominates the behavior of the FWM signal for excitation at the exciton resonance, those contributions are unimportant in the case of the continuum.

In the last part of this subsection, we discuss implications of the spatial dynamics on dephasing. We have shown that the polarization extends over macroscopic distances if, for large time delays, a photon echo is generated from continuum states of a semiconductor. This may have important consequences for the dephasing time measured in a TI FWM experiment. It is plausible that excitations with a large size are more likely to dephase than smaller ones because of the higher probability of interaction between them as well as with "defects" present in a real crystal. In fact, the excitonic polarization, which occupies a small volume in space, dephases on a picosecond time scale,[24] whereas the spatially larger polarization of continuum states dephases on the time scale of 100 fs.[25]

C. Influence of dispersion

In the last subsection, we have found that the spatially resolved electron-hole-pair amplitude occupies a large volume if continuum states are excited. The spatial extent of the polarization is already of the order of the wavelength of the exciting pulses for typical material parameters. This raises the question whether the finite wavelength of the light can still be neglected.

An exact solution for the third-order polarization can be found for noninteracting particles, solving the equation of motion for the two-point density matrix. Assuming a pulse of the form (3), the $\mathbf{K}$th Fourier component of the third-order polarization, proportional to $E_2^2\,E_1^*$, is given by

$$P_{\mathbf{K}}^{(3)}(t) = -\delta_{\mathbf{K}\,2\mathbf{K}_2-\mathbf{K}_1}\,\frac{|\mu|^4}{(i\hbar)^3}\,\frac{1}{(2\pi)^3}\int d^3k \int_{-\infty}^{+\infty} dt_3 \int_{-\infty}^{+\infty} dt_2 \int_{-\infty}^{+\infty} dt_1\, E_2(t_3)\,E_2(t_2)\,E_1^*(t_1) \tag{9}$$
$$\times e^{-i\,\omega_c(2\mathbf{K}_2-\mathbf{K}_1+\mathbf{k})\,(t-t_2)}\,e^{-i\,\omega_v(\mathbf{K}_2-\mathbf{K}_1+\mathbf{k})\,(t_2-t_1)}\,e^{-i\,\omega_c(\mathbf{K}_2+\mathbf{k})\,(t_1-t_3)}\,e^{-i\,\omega_v(\mathbf{k})\,(t_3-t)}\,.$$

Here, $\hbar\omega_{c,v}(\mathbf{k}) = \hbar^2k^2/(2\,m_{c,v})$ is the dispersion of the conduction and valence band, respectively. Equation (9) shows that the FWM signal is emitted only in the direction $2\,\mathbf{K}_2 - \mathbf{K}_1$, due to momentum conservation.

In $\mathbf{k}$ space, the first-order polarizations of the first and second pulse, $\tilde{\psi}_{1,2}^{(1)}(\mathbf{k})$, differ by the vector $\mathbf{K}_2 - \mathbf{K}_1$. Assuming $\mathbf{K}_2 - \mathbf{K}_1 = \mathbf{0}$ Eq. (5) follows, where the energy $\hbar\omega^{(\lambda)}$ has to be replaced by the energy $\hbar\omega(\mathbf{k}) = \hbar\omega_c(\mathbf{k}) - \hbar\omega_v(\mathbf{k}) + \hbar^2\,K_1^2/(2m_e + 2m_h)$ of the interband transition.

The above approximation is valid if $\mathbf{K}_1 - \mathbf{K}_2$ is much smaller than the correlation length of the first-order polarization in $\mathbf{k}$ space. By virtue of the sampling theorem, this is equivalent to $2\pi/|\mathbf{K}_1 - \mathbf{K}_2| \gg d$, where d is the di-

ameter of the first-order polarization in real space. This is a much weaker condition than the condition that the wavelength of the light itself has to be much larger than d. The weaker condition is fulfilled in all practical cases, and there is no influence of the finite wavelength on the FWM signal, apart from the tiny change of the transition energy, which is irrelevant in the limit of a constant absorption coefficient in the region of interest.

An analytical solution cannot be given for interacting particles. If excitonic states are excited, the characteristic extent d is of the order of the exciton Bohr radius, as demonstrated by the numerical results in Figs. 2 and 3. Hence, we are in the limit $2\pi/K_1 = 2\pi/K_2 \gg d$, so that the finite wavelength can be neglected. For excitation of the continuum, we make use of the fact that the first-order polarization of the interacting system is proportional to the solution for free particles as found in the last subsection. Therefore, the above result for free particles can be applied, i. e., the finite wavelength of the excitation light can be neglected as well. In summary, the above discussion shows that, both for interacting and noninteracting particles, and for all excitation conditions treated in this paper, the finite wavelength of the exciting pulses is negligible in spite of the large spatial extent of the polarization.

IV. CONCLUSIONS

We have investigated the spatial and temporal dynamics of the electron-hole-pair amplitude generated in FWM experiments in a semiconductor for excitation at the exciton resonance, between the exciton and the band edge, and far in the continuum. In all cases, we find that the spatial dynamics of the polarization reflect the temporal dynamics of the FWM signal.

The first-order and the third-order polarization of the exciton are confined to a narrow region around $\mathbf{r} = \mathbf{0}$, where $\mathbf{r}$ is the relative coordinate between electron and hole. The third-order polarization is created at $\mathbf{r} = \mathbf{0}$ and, consequently, the TR FWM signal starts immediately after the excitation. The rise of the TR FWM is slow, due to polarization interference.

The FWM signal is emitted as photon echo for excitation of continuum states, i. e., it is delayed in time with respect to the exciting pulses. The spatial dynamics are characterized by expansion and contraction of wave packets. The time delay with which the photon echo is emitted equals the time the third-order polarization needs to propagate to $\mathbf{r} = \mathbf{0}$, where it can be monitored in an optical experiment.

Our results demonstrate that the polarization, in the case of continuum excitation, can occupy a volume in space that is larger than the typical wavelength of the exciting light. Therefore, we have explicitly verified that it is still valid to neglect the finite wavelength of the exciting light in this situation.

We have shown that the photon echo from semiconductor continuum states has essentially the same dynamic properties as the photon echo from a system of noninteracting particles where Coulomb interaction is neglected. This is due to the fact that both the first-order and the third-order polarization in a semiconductor for continuum excitation differ only by a constant complex factor from the results for a noninteracting system. Therefore, the photon echo from semiconductor continuum states has a much larger amplitude than the one from the noninteracting system, but the temporal shape and the temporal position of the echo pulse are almost the same as in the noninteracting case. The shape and position are determined by the solution for independent two-level systems. We conclude that polarization interference does not significantly change the dynamics in FWM experiments for excitation of the semiconductor continuum, in contrast to the results for excitons. The intensity of the photon echo from semiconductor band states, however, is considerably enlarged by Coulomb enhancement.

ACKNOWLEDGMENTS

The authors are indebted to S. Bar-Ad and K. El Sayed for stimulating discussions. This work was supported by the Director, Office of Energy Research, Office of Basic Energy Sciences, Division of Material Sciences of the U.S. Department of Energy, under Contract No. DE-AC03-76SF00098. One author (S. G.) wishes to thank the Deutsche Forschungsgemeinschaft for financial support.

* Permanent address: Swiss Federal Institute of Technology (ETH), Institute of Quantum Electronics, Hönggerberg, 8093 Zürich, Switzerland.

[1] N. A. Kurnitt, I. D. Abella, and S. R. Hartmannn, Phys. Rev. Lett. **13**, 567 (1964).
[2] G. Noll, U. Siegner, S. G. Shevel, and E. O. Göbel, Phys. Rev. Lett. **64**, 792 (1990).
[3] U. Siegner, D. Weber, E. O. Göbel, D. Bennhardt, V. Heuckeroth, R. Saleh, S. D. Baranovskii, P. Thomas, H. Schwab, C. Klingshirn, J. M. Hvam, and V. G. Lyssenko, Phys. Rev. B **46**, 4564 (1992).
[4] D. Bennhardt, P. Thomas, A. Weller, M. Lindberg, and S. W. Koch, Phys. Rev. B **43**, 8934 (1991).
[5] L. Schultheis, M. D. Sturge, and J. Hegarty, Appl. Phys. Lett. **47**, 995 (1985).
[6] M. D. Webb, S. T. Cundiff, and D. G. Steel, Phys. Rev. Lett. **66**, 934 (1991); Phys. Rev. B **43**, 12 658 (1991).
[7] T. Yajima and Y. Taira, J. Phys. Soc. Jpn. **47**, 1620 (1979).
[8] H. Haug and S. W. Koch, *Quantum Theory of the Optical and Electronic Properties of Semiconductors*, 2nd ed. (World Scientific, Singapore, 1993), and references therein.
[9] M. Lindberg, R. Binder, and S. W. Koch, Phys. Rev. A **45**, 1865 (1992).
[10] Y. Z. Hu, R. Binder, and S. W. Koch, Phys. Rev. B **47**, 15 679 (1993).
[11] F. Jahnke, M. Koch, T. Meier, J. Feldmann, W. Schäfer,

P. Thomas, S. W. Koch, E. O. Göbel, and H. Nickel, Phys. Rev. B **50**, 8114 (1994).
[12] A. Lohner, K. Rick, A. Leitensdorfer, T. Elsaesser, T. Kuhn, F. Rossi, and W. Stolz, Phys. Rev. Lett. **71**, 77 (1993).
[13] D.-S. Kim, J. Shah, J. E. Cunningham, T. C. Damen, S. Schmitt-Rink, and W. Schäfer, Phys. Rev. Lett. **68**, 2838 (1992).
[14] H. J. Bakker and H. Kurz, Phys. Rev. B **50**, 7805 (1994).
[15] M. Wegener, D. S. Chemla, S. Schmitt-Rink, and W. Schäfer, Phys. Rev. A **42**, 5675 (1990).
[16] K. Leo, M. Wegener, J. Shah, D. S. Chemla, E. O. Göbel, T. C. Damen, S. Schmitt-Rink, and W. Schäfer, Phys. Rev. Lett. **65**, 1340 (1990).
[17] W. Schäfer, F. Jahnke, and S. Schmitt-Rink, Phys. Rev. B **47**, 1217 (1993).
[18] S. Weiss, M.-A. Mycek, J.-Y. Bigot, S. Schmitt-Rink, and D. S. Chemla, Phys. Rev. Lett. **69**, 2685 (1992).
[19] D.-S. Kim, J. Shah, T. C. Damen, W. Schäfer, F. Jahnke, S. Schmitt-Rink, and K. Köhler, Phys. Rev. Lett. **69**, 2725 (1992).
[20] J. Feldmann, T. Meier, G. von Plessen, M. Koch, E. O. Göbel, P. Thomas, G. Bacher, C. Hartmann, H. Schweizer, W. Schäfer, and H. Nickel, Phys. Rev. Lett. **70**, 3027 (1993).
[21] T. Rappen, U. Peter, M. Wegener, and W. Schäfer, Phys. Rev. B **48**, 4879 (1993).
[22] O. Madelung and W. Kress, in *Physics of Group IV Elements and III-V Compounds*, edited by O. Madelung, M. Schulz, and H. Weiss, Landolt-Börnstein, New Series, Group III, Vol. 17, Pt. a (Springer, Berlin, 1982), p. 158.
[23] R. J. Elliott, Phys. Rev. **108**, 1384 (1957); R. Zimmermann, Phys. Status Solidi B **135**, 681 (1986); P. Lefebvre, P. Christol, and H. Mathieu, Phys. Rev. B **48**, 17 308 (1993).
[24] L. Schultheis, J. Kuhl, A. Honold, and C. W. Tu, Phys. Rev. Lett. **57**, 1635 (1986).
[25] P. C. Becker, H. L. Fragnito, C. H. Brito Cruz, R. F. Fork, J. E. Cunningham, J. E. Henry, and C. V. Shank, Phys. Rev. Lett. **61**, 1647 (1988).